Membrane Mechanics of Glass-Bilayer Adhesion in a Pipette

Tristan Ursell, Ashutosh Agrawal, and Rob Phillips
Department of Applied Physics, California Institute of Technology, Pasadena, CA

March 17, 2011

Abstract

Electrophysiology is a central tool for measuring how different driving forces (e.g. ligand concentration, transmembrane voltage, or lateral tension) cause a channel protein to gate. Upon formation of the high resistance seal between a lipid bilayer and a glass pipette, the so-called 'giga-seal', channel activity can be recorded electrically. In this paper, we explore the implications of giga-seal formation on the mechanical state of the membrane patch. We employ a mechanical model for the free energy of membrane geometry in the presence of glass-bilayer adhesion to draw two potentially important conclusions. First, we use our adhesion model to derive an explicit relationship between applied pressure and patch shape that is consistent with the Laplace-Young Law, giving an alternative method of calculating patch tension under pressure. With knowledge of the adhesion constant, which we find to be in the range $\sim 0.1 - 1\, k_B T/\mathrm{nm}^2$, and the pipette size, one can precisely calculate the patch tension as a function of pressure, without the difficultly of obtaining an optical measurement of the membrane radius of curvature. Second, we employ data from previous electrophysiological experiments to show that over a wide range of lipids, the resting tension on a electrophysiological patch is highly variable and can be 10-100 times higher than estimates of the tension in a typical cell membrane. This suggests that electrophysiological experiments may be systematically altering channel gating characteristics and querying the channels under conditions that are not the same as their physiological counterparts.

1 Introduction

The use of pipettes to hold and deform both model and biological membranes is a key part of the experimental repertoire of modern membrane biophysics [1, 2, 3, 4, 5, 6]. Electrophysiology is a powerful and well-accepted technique for the quantification of ion channel gating in a variety of chemical and physical settings [7, 8, 9, 10]. In some cases, the set of possible ion channel conformations depends both on which molecules are present (e.g. ligands) and the physical state of the bilayer (e.g. bilayer thickness, curvature, or lateral tension) [11]. In particular, some channels uniquely respond to their physical environment, and furthermore, it has been argued that lateral tension affects the gating of any ion channel that changes its areal footprint or hydrophobic thickness during a conformational change [8, 12, 13, 14]. Likewise, extreme conditions (e.g. very high salt concentration, very stiff bilayers, or high lateral tension) might cause some physiologically relevant channel conformations to be disfavored, while favoring conformations that are not usually adopted under physiological circumstances. With these facts in mind, this paper examines how the intrinsic interaction between a lipid bilayer and glass leads to resting tensions within a pipette that can be one or two orders of magnitude larger than the resting tension on a typical living cell membrane [15]. Using linear elasticity theory, we calculate the bilayer patch shape and lateral tension in the presence of an applied suction pressure in the pipette. These calculations reveal a route to

determine membrane tension without knowledge of patch curvature. We compare this calculation with previous experimental results, which suggests that there is a relatively large variability in the strength of bilayer-glass adhesion, and hence a large variability in the resting tension on the bilayer during electrophysiological experiments.

2 Bilayer Tension during Giga-seal Formation

As a prerequisite to calculating the relationships between pressure, membrane geometry, and tension, we first calculate the resting tension on a membrane that has adhered to a glass pipette in the absence of an applied suction pressure. In all of the calculations that follow in this paper, we make a number of simplifying mechanical assumptions about the bilayer. First, we assume that the behavior of the system is determined by lipid bilayer mechanics alone; we do not account for the effects of any structural or cytoskeletal components. Second, we assume that the total amount of lipid in the adhered and free-standing regions is constant, and that the adhesion of the bilayer along the glass is uniform and smooth, such that there are no folds, ripples, or extraneous sources of lipids that are not either part of the adhered zone or the free-standing region within the pipette. Third, for the magnitudes of adhesion strength and pressure considered here, we assume that the contributions to bilayer energetics from mean curvature bending are negligible, an assumption that is motivated and explored in the Discussion section. Fourth, we assume that the bilayer is a linear elastic material that has a stretch modulus $K_A \simeq 50\, k_B T/\mathrm{nm}^2$ [16], and a linear relationship between the areal strain, ϕ, and the lateral tension, τ, given by $\tau = K_A \phi$. Finally, we assume that contact between the glass and the membrane lowers the mechanical free energy and, simultaneously, that when adhered, the membrane is free to slide along the glass without incurring any energy cost (*i.e.* the contact is frictionless). These last two assumptions ensure that the tensions in the adhered and free-standing regions of the membrane are equal.

For the purposes of discussion, we consider a right cylindrical pipette as shown in Fig. 1. However, we emphasize that for all of the analysis that follows, our calculations apply to any pipette shape, so long as the radius is constant in the region where the membrane transitions from the adhered region to the free-standing region (e.g. a cylindrical pipette with a tapered or bent tip). We define the adhered region as the domain adhered to the interior of the pipette, and we define the free-standing region as the circular domain with radius R_p. Since the total amount of lipid in the two regions is conserved, this implies that the initial unstressed area is related to the final stressed area, such that we can write

$$(1+\phi)A_o = A_{\mathrm{adh}} + \pi R_p^2, \tag{1}$$

where A_o is the the total, unstressed area of membrane in the adhered and free-standing regions and A_{adh} is the area of the adhered region. The unstressed area is related to the number of lipids in the system by $A_o = n a_o$, where n is the number of lipids and a_o is the area per lipid in the unstressed state. The areal strain in the bilayer, ϕ, stores an elastic stretch energy

$$G_{\mathrm{str}} = A_o \frac{K_A}{2} \phi^2. \tag{2}$$

Glass-bilayer adhesion is incorporated into the model through a phenomenological energy $G_{\mathrm{adh}} = -\gamma A_{\mathrm{adh}}$, where γ is the strength of adhesion and $A_{\mathrm{adh}} = 2\pi R_p L_o$ for the particular membrane configuration shown in Fig. 1(a). The adhesion energy can be re-written as

$$G_{\mathrm{adh}} = -\gamma \left((1+\phi)A_o - \pi R_p^2 \right), \tag{3}$$

using eqn. 1, and hence does not depend on the shape of the adhered region so long as R_p remains constant. The total mechanical free energy is the sum of the stretch and adhesion energies of the membrane, given by

$$G = G_{\text{str}} + G_{\text{adh}} = A_o \frac{K_A}{2}\phi^2 - \gamma\left((1+\phi)A_o - \pi R_p^2\right). \tag{4}$$

Minimization of this energy with respect to the areal strain, ϕ, yields the equilibrium value $\phi = \gamma/K_A$, and hence the lateral tension $\tau = \gamma$ in both the adhered and free-standing membrane regions, independent of the shape of the adhered region. This result shows that the resting lateral tension in the patch is determined only by the glass-bilayer adhesion strength, not by any geometric factors describing the patch or pipette. Later in this paper we determine values for the adhesion coefficient, γ, that indicate that resting tensions due to adhesion may be orders of magnitude larger than the typical resting tension of a bilayer under physiological conditions.

3 Bilayer Tension Under Pressure

When a pressure gradient is applied across the membrane, the geometry of the membrane changes to accommodate the energetic interplay between pressure and volume, such that the free-standing bilayer region adopts a dome-like shape with a finite curvature [7, 12], as shown in Fig. 1(b). We assume that this shape is described by a chord of a sphere, with a radius of curvature R_c and a polar angle θ, restricted by geometry to be

$$\theta = \sin^{-1}(\rho), \tag{5}$$

where the term in parentheses, $\rho = R_p/R_c$, is a dimensionless measure of the curvature for the free-standing spherical domain. In the limit of vanishing pressure, when the free-standing region tends toward a planar configuration, $R_c \to \infty$ and $\rho \to 0$. In contrast, for high values of applied pressure, when the free-standing membrane tends toward a shape with maximum allowable curvature, $R_c \to R_p$ and $\rho \to 1$. For any shape that the free-standing region adopts between these two bounds, its area is given by

$$A_f = 2\pi R_c^2(1-\cos\theta) = \frac{2\pi R_p^2}{\rho^2}(1-\sqrt{1-\rho^2}). \tag{6}$$

Since the total amount of lipid in both regions is conserved, we can again relate the current parameters that describe the membrane shape to the amount of unstressed area and the areal strain, ϕ, felt throughout the membrane, by the relationship

$$(1+\phi)A_o = A_{\text{adh}} + \frac{2\pi R_p^2}{\rho^2}(1-\sqrt{1-\rho^2}), \tag{7}$$

where for the cylindrical pipette shown in Fig. 1(b), $A_{\text{adh}} = 2\pi R_p L_p$ and L_p is the length of the adhered region under pressure. Again, the shape of the adhered region is unimportant as long as R_p remains constant in the transition zone between the adhered and free standing regions. This equation can be rearranged to give an expression for the adhered area as a function of areal strain, ϕ, and patch curvature, ρ,

$$A_{\text{adh}} = (1+\phi)A_o - \frac{2\pi R_p^2}{\rho^2}(1-\sqrt{1-\rho^2}). \tag{8}$$

In addition to altering the amount of adhered area, the application of pressure increases the membrane-enclosed volume relative to the zero-pressure state by an amount

$$\Delta V = \pi R_p^2(L_p - L_0) + \frac{\pi}{3}R_c^3(1-\cos\theta)^2(2+\cos\theta), \tag{9}$$

due to both the areal strain of the membrane and the deformation of the free-standing region into a dome-like shape. Using eqns. 5 and 7, eqn. 9 can be expressed as a function of the dimensionless curvature, ρ, and areal strain ϕ.

Incorporating the contributions from membrane stretch, glass-bilayer adhesion, and pressure-volume coupling, the expression for the total free energy of the membrane under pressure is

$$G(\phi, \rho) = A_o \frac{K_A}{2} \phi^2 - \gamma A_{\text{adh}}(\phi, \rho) - p\Delta V(\phi, \rho). \tag{10}$$

In contrast to the free energy at zero pressure, this free energy depends on two, independent *variables*, namely the areal strain, ϕ, and the dimensionless curvature ρ; whereas the pipette size R_p, pressure p, and adhesion constant γ are fixed *parameters*. In this situation mechanical equilibrium is found by minimizing the free energy with respect to ϕ and ρ simultaneously.

Minimization of G with respect to ϕ yields the equilibrium value of the areal strain $\phi = (\gamma + pR/2)/K_A$. Multiplication of the areal strain with the stretch modulus gives the membrane tension under pressure

$$\tau = \gamma + \frac{p\,R_p}{2}. \tag{11}$$

Equation 11 shows that the tension has a linear relationship to the adhesion strength, and has a separate linear dependence on the the applied pressure. Note that the tension does not depend on the amount of adhered area, nor the radius of curvature of the free-standing region. This means that if one performs a set of calibration experiments to determine the glass-bilayer interaction energy (as discussed in section 4), and then measures the pipette radius and the applied pressure, one knows the lateral tension without any measurements of patch curvature.

Minimization of the free energy in eqn. 10 with respect to the dimensionless curvature ρ yields

$$\frac{\pi R_p^2}{\rho^4\sqrt{1-\rho^2}}[-2+\rho^2+2\sqrt{1-\rho^2}]\,(p(\rho-1)R_p+2\gamma\rho)=0, \tag{12}$$

for which either the term in square brackets or the term in parentheses is zero. Setting the term in the square brackets to zero yields the trivial solution $\rho = 0$, whereas setting the latter term to zero gives

$$\rho = \frac{p\,R_p}{p\,R_p + 2\gamma}. \tag{13}$$

This equation makes a connection between the curvature of the free-standing region and applied pressure. Whereas normally, one must measure the curvature at each pressure to determine tension, we have derived a mechanical relationship that allows one to accurately calculate the curvature as a function of pressure. Conversely, one can rearrange this equation to

$$R_c = R_p + \frac{2\gamma}{p}, \tag{14}$$

and use it as a tool to calibrate subsequent measurements. Specifically, by measuring the curvature of the free-standing region as a function of pressure, one can fit this equation to find the adhesion coefficient, γ, for a particular type of lipid and thus use eqn. 11 to find the tension in any subsequent experiment where the pipette size is known. Combining our eqns. 11 and 14 yields the familiar Laplace-Young Law, $\tau = pR_c/2$, demonstrating that these are consistent formulations.

In addition to the dimensionless curvature ρ, the parameters in eqns. 11 and 13 can be arranged to yield a dimensionless tension $\hat{\tau} = \tau/\gamma$ and a dimensionless pressure $\hat{p} = pR_p/2\gamma$. With these

three dimensionless parameters, eqns. 11 and 13 reduce to universal, parameter-free forms, given by

$$\hat{\tau} = 1 + \hat{p} \quad \text{and} \quad \rho = \frac{\hat{p}}{1+\hat{p}}. \tag{15}$$

Figure 2 shows plots of $\hat{\tau}$ and ρ as a function of the dimensionless pressure $\hat{p}$, to illustrate the functional form of these curves.

Our model also predicts that as pressure is applied and the dome-like shape in the free-standing region appears, the membrane stretches, and the proportion of lipids in the adhered region decreases, while the proportion of lipids in the free-standing region increases, with the total amount of lipid conserved. We can couch this mathematically as the amount of lipid in the free-standing region at a given (dimensionless) pressure relative to the original amount of lipid in the free-standing region at zero pressure, given by

$$\begin{aligned} \Delta A_f &= \frac{(A_f/(1+\phi))|_p - (A_f/(1+\phi))|_{p=0}}{(A_f/(1+\phi))|_{p=0}} \\ &= 2\frac{((1+\hat{p})/\hat{p})^2}{1+\hat{p}\frac{\phi_o}{1+\phi_o}}\left(1-\sqrt{1-(\hat{p}/(1+\hat{p}))^2}\right) - 1, \end{aligned} \tag{16}$$

where $\phi_o = \gamma/K_A \simeq 0.01$ is the areal strain of the membrane at zero pressure, and the factor $1/(1+\phi)$ relates the stressed membrane area to the unstressed area, and hence to the amount of lipid. This effect occurs because it is energetically favorable to remove lipids from the adhered region at a fixed cost per unit area, and add them to the dome-like, free-standing region where they increase the membrane-enclosed volume that couples to the applied pressure. For a fixed protein to lipid ratio, this increase in the amount of lipid in the free-standing region may also translate to a proportional increase in the amount of protein found in the free-standing region, and hence an increase in the number of measurable channels. In such a situation, the total number of channels as a function of applied pressure is given by

$$N(\hat{p}) = c\frac{\pi R_p^2}{a_o(1+\phi_o)}\left(1+\Delta A_f\right), \tag{17}$$

where N is the number of channel proteins in the free-standing region, a_o is the area per lipid molecule, and c is the protein to lipid number ratio. At high pressures, where the areal strain is $\sim 3-4\%$, this increase in free-standing membrane, and the corresponding increase in measurable proteins, can be as large as $\sim 20\%$, as shown in Fig. 3(a). For example, non-interacting channels that each individually have a dose-response as a function of pressure $P(\hat{p})$, would have a population dose-response proportional to $N(\hat{p})P(\hat{p})$. Thus in the absence of any intrinsic mechanosensitivity, a population of channels may appear mechanosensitive, via a response to applied pressure, simply because the number of measurable channels increases as pressure increases.

Finally, as the membrane stretches and lipids leave the adhered region to join to the free-standing region, one can use eqns. 7 and 15 to calculate that the point of contact between the adhered and free-standing regions translates along the pipette. The degree of translation and even the direction of the translation depend on the total amount of lipid in the system, dictated by the area ratio $A_o/\pi R_p^2$. These effects are demonstrated in Fig. 3(b).

4 Measuring Adhesion Strength from Membrane Curvature

Using data from multiple lipid mixtures and preparations that link curvature of the free-standing region to applied pressure, we calculated the glass-bilayer adhesion energy, γ, though as is evident

below, the adhesion strength shows significant variation. As part of their study to understand the gating of the mechanosensitive channel MscL [7], Moe and Blount obtained measurements of patch curvature as a function of applied pressure. Their data can be used to fit eqn. 14 for the adhesion energy and the pipette radius R_p. Ideally, if all pipette and lipid preparations were identical, all of the lines associated with a particular lipid type would have the same slope, and only the pipette radius would change from one experiment to the next. However, the variability in our fits suggests that things may not be so simple. There are a number of potential ways that the interaction between glass and bilayer may be altered, for instance pH drift in the recording buffer [17, 18], slight variations in glass composition and surface roughness, or changes in adhered lipid composition.

We performed this linear fit on the data to extract the adhesion energy for the different lipid mixtures. Our fitting results are summarized in Figs. 4 and 5. Some lipid mixtures show fairly homogeneous values of the adhesion energy, while others span a factor of two or three. Across all lipid types, the mean bilayer-glass adhesion energy was estimated to be $0.54 \pm 0.31\, k_BT/\text{nm}^2$. In a similar study, Opsahl and Webb [19] also reported values with a wide range of $\gamma = 0.12 - 0.97\, k_BT/\text{nm}^2$. Interestingly, when using the data published in their paper, our model gives a slightly different result, specifically from their Fig. 3 they calculate $\gamma = 0.63\, k_BT/\text{nm}^2$, whereas we calculate $\gamma = 0.47\, k_BT/\text{nm}^2$. This difference stems from the way Opsahl and Webb incorporate the effects of adhesion into their model. They assume that the adhesion forces, which act normal to the contact surface, exhibit a maximum value T_a. At the point of contact between the free-standing region and the pipette, this maximal force in the adhered region is balanced by the component of the membrane tension in the free-standing region that acts perpendicular to the pipette surface. This force balance equation, along with the Laplace-Young Law for the free-standing region and a geometric relation similar to eqn. 5, results in the relationship

$$R_c^2 = R_p^2 + 4T_a^2/p^2. \tag{18}$$

To make a comparison with this expression, we square the two sides of eqn. 14 to obtain

$$R_c^2 = R_p^2 + 4\gamma^2/p^2 + 4\gamma R_p/p. \tag{19}$$

Considering γ to be equal to T_a, the difference between the two relations is restricted to the term $4\gamma R_p/p$. We can use the same dimensionless parameters employed previously to cast the differences between these two methods in a more illuminating light. As noted earlier, this work found that the dimensionless tension and pressure were related by $\hat{\tau} = 1 + \hat{p}$, whereas Opsahl and Webb find that $\hat{\tau} = \sqrt{1 + \hat{p}^2}$. The differences in these two formulations are shown in Fig. 2(a).

5 Applications to Mechanosensitive Channels

In patch clamp experiments with reconstituted mechanosensitive channels, varying the pressure across the membrane results in increased membrane tension that gates the channels. Both theoretical models and careful experimental studies have successfully established the functional dependence of channel gating on the tension in the lipid membrane. However, to further our understanding of the gating mechanisms of these channels it would be useful to connect the applied pressure to the corresponding tension in the membrane without the tedious imaging usually required to measure the curvature of the free-standing region. To this end, below we examine available data from the experiments on mechanosensitive channels using (i) the Laplace-Young Law, (ii) the formulation of Opsahl and Webb, (iii) and the formulation developed in this work.

Method 1: As shown earlier, the two equilibrium eqns. 11 and 14 obtained from energy minimization together yield the Young-Laplace relation, $\tau = pR_c/2$, for the free-standing membrane

region. If the membrane curvature is known along with the pressure, this relation provides the most straightforward approach to compute the lateral tension. In their study of MscL gating, Moe and Blount [7] used the Laplace-Young Law to calculate the gating probability of the channel as a function of membrane tension. However, in general, due to the challenges associated with obtaining optical data on the membrane curvature, this approach has limited applicability.

Method 2: If optical data of membrane curvature is lacking, the approach of Opsahl and Webb can be used to calculate the radius of curvature of the free-standing membrane region. As discussed in sec. 4, the radius of curvature is given by $R_c = \sqrt{R_p^2 + 4\gamma^2/p^2}$, and substituting this expression into the Young-Laplace relation yields $\tau = \sqrt{\gamma^2 + (pR_p/2)^2}$. Thus, with knowledge of the pipette radius and the adhesion energy, one can calculate the membrane tension from this expression.

Method 3: For the same scenario where the curvature of the free-standing region is not known, a measure of the tension can be obtained from eqn. 11, $\tau = \gamma + pR_p/2$, derived earlier. This is equivalent to the substitution of eqn. 14 into the Young-Laplace relation. Similar to method 2, an estimate of the adhesion energy and the pipette radius are required to calculate membrane tension. However, in contrast to the relation presented in method 2, in this method membrane tension exhibits a linear dependence on adhesion energy, pipette size, and pressure.

Comparing the tensions calculated from method 2 ($\hat{\tau}_2$) and method 3 ($\hat{\tau}_3$), we note that for higher values of $\hat{p}$ both methods increase in a manner $\propto \hat{p}$, as shown in Fig. 2(a), and the relative difference in tension between the two methods, $2(\hat{\tau}_2 - \hat{\tau}_3)/(\hat{\tau}_2 + \hat{\tau}_3)$, decreases like $\hat{p}^{-1}$. We employ the approaches discussed above to estimate the gating tension of the mechanosensitive channel of large conductance (MscL) from experiments that use three different lipid bilayers: PC16, PC18, and PC20, with acyl chain lengths of 16, 18 and 20 carbons, respectively. This study by Perozo et al. [10] estimated the applied pressure for the opening of a MscL channel to be around 24 mm Hg, 42 mm Hg and 72.7 mm Hg, respectively. Due to the lack of available data on membrane curvature, we employ methods 2 and 3 to estimate the gating tensions for the three different lipid types, and present these results in Table 1. To make these estimates, we assume an average adhesion energy of $0.9\,k_BT/\text{nm}^2$ for pure PC bilayers, as suggested by Fig. 5, and a pipette radius of $1\,\mu m$. For comparison, Moe and Blount [7] estimated the gating tension at $\sim 2.5\,k_BT/\text{nm}^2$ for a MscL channel reconstituted in DOPC/DOPS (1:1).

6 Discussion

Although a general consensus about the value of resting tension in cell membranes is lacking, a few studies have estimated it to be in the range of $\sim 0.001 - 0.01\,k_BT/\text{nm}^2$ [15, 20, 21]. On average we calculated the membrane tension induced by adhesion of the bilayer to a glass pipette to be $\sim 0.5\,k_BT/\text{nm}^2$, thus, our work indicates that channel proteins reconstituted into lipid bilayers that are adhered to a pipette are subject to lateral tensions significantly higher than those found in cell membranes. Considering that many channels that were thought to be strictly voltage-gated channels respond in a non-trivial way to membrane tension [8, 14, 22, 23], and the fact that tension has been shown to alter the available conformational states of some channels [24], we wonder whether this large resting tension in patch clamp experiments relative to those found in cells is systematically affecting a broad class of electrophysiological measurements.

In this work, we used linear elasticity to calculate the lateral tension in a lipid bilayer adhered onto a pipette during electrophysiological experiments. For simplicity, we neglected the contributions of bending energy to the total system energy. A simple comparison of the orders of magnitude of the different energies justifies this approximation. For the case of vanishing applied pressure, a conservative estimate of the adhesion energy per unit unstressed area is $-\gamma\phi$ which is approx-

imately $-5 \times 10^{-3}\, k_B T/\mathrm{nm}^2$ for $\gamma \approx 0.5\, k_B T/\mathrm{nm}^2$. The stretch energy per unit initial area is given by $K_A \phi^2/2$ and is calculated to be around $2.5 \times 10^{-3} k_B T/\mathrm{nm}^2$ for $K_A \approx 50\, k_B T/\mathrm{nm}^2$. The bending energy of the bilayer per unit area is given by $2\kappa_b H^2$, where κ_b is the bending modulus of the bilayer. The cylindrical section has a mean curvature of $H = 1/2R_p$ while the spherical patch has a maximum mean curvature of $H = 1/R_p$, and hence, for a typical value of $\kappa_b \approx 20\, k_B T$ and $R_p \approx 1\, \mu m$, these contributions are approximately $10^{-5} k_B T/\mathrm{nm}^2$ which is two orders of magnitude smaller than the adhesion and stretch energies, and hence can be safely neglected.

The areal strain of a membrane under arbitrary pressure can be calculated by knowing the stretch modulus of the bilayer, $K_A \simeq 50\, k_B T/\mathrm{nm}^2$, and the lateral tension on the membrane (eqn. 11). Using average values of the adhesion strength ($\gamma \simeq 0.5\, k_B T/\mathrm{nm}^2$) and stretch modulus, the areal strain of the membrane is $\sim 1\%$ at zero pressure. During electrophysiological experiments, the applied pressure is of order one tenth of an atmosphere or $p = 0.001\, k_B T/\mathrm{nm}^3$, and the pipette radius is $\sim 1\, \mu m$, leading to an areal strain of $\sim 2\%$. Although membrane rupture is a stochastic process [25], the approximate maximum strain that a membrane can typically endure is approximately $3 - 4\%$ [26]. Thus, in the presence of adhesion and pressure, the membrane is in the vicinity of its failure point. In addition, studies have linked the strength of glass-bilayer adhesion to increased giga-seal resistance [17] and hence decreased noise in electrophysiological measurements. These facts suggest a fundamental trade-off between patch life-time and measurement noise; patches that adhere more tightly to the glass form a better giga-seal but fail more quickly due to stochastic rupture. Likewise, eqn. 11 shows that the areal strain is directly proportional to the pipette radius, implying that for a given pressure, a larger pipette radius would generate higher areal strain and membrane tension, thus enhancing the risk of membrane rupture.

The topic of bilayer-substrate adhesion has been an area of lively research, and as such we conclude with a few related remarks to put this work into a larger context. Adhesion is often studied using constant volume vesicles where adhesion strength can be determined from vesicle shape constraints [27]. However, in electrophysiological membranes we have employed the complementary constant pressure ensemble. Additionally, while membrane adhesion is often mediated indirectly by proteins, the adhesion we consider here involves the binding of individual lipids to glass, and hence tends to be significantly stronger than protein-mediated adhesion. For example, Seifert and Lipowsky [28] modeled the morphology of vesicles weakly adhered to substrates with $\gamma \approx 10^{-6} - 10^{-5}\, k_B T/\mathrm{nm}^2$, and Smith *et al.* [29] studied the pulling of tethers in vesicles adhered to rigid substrates for adhesion strengths around $10^{-3}\, k_B T/\mathrm{nm}^2$. Experimentally, Smith *et al.* [30] used magnetic tweezers to study the force-deflection of vesicles with protein-mediated adhesion, finding $\gamma \approx 10^{-5}\, k_B T/\mathrm{nm}^2$. Our estimate of the average adhesion strength, as well as estimates from bilayers [19] and even from different types of cell surfaces [31], suggest that direct binding of lipid on glass is a significantly stronger form of adhesion, on the order of $\gamma \simeq 0.5\, k_B T/\mathrm{nm}^2$. Furthermore, our calculations based on the experimental data of Perozo *et al.* [10], indicate that applied pressure and adhesion are each contributing approximately equally to the net tension required to gate certain mechanosensitive channels in an electrophysiological experiment. The fact that the resting tension comprises a significant portion of the gating tension, even for large mechanosensitive channels (e.g. MscL), together with the fundamental trade off between adhesion strength and measurement noise, indicates the existence of an electrophysiological blind spot. Any channel that has conformational changes sensitive to tensions below $\sim 0.5\, k_B T/\mathrm{nm}^2$ would be inaccessible to electrophysiology, yet it is precisely this lower tension regime $\ll 0.5\, k_B T/\mathrm{nm}^2$ that seems physiologically relevant for a broad range of cellular membranes.

7 Conclusion

In this work we used a linear elastic model and data from previous experiments on mechanosensitive channels to gain a better understanding of how glass-bilayer adhesion affects the mechanical state of a membrane patch during an electrophysiological experiment. We derived an alternative method for calculating membrane tension that does not rely on imaging the membrane, but does require knowledge of the adhesion strength and pipette size. We used this to calculate the adhesion strength across multiple lipid types and found that it is highly variable, and that adhesion causes the resting tension, in the absence of applied pressure, to be orders of magnitude higher than estimated physiological tensions. Additionally, applied pressure causes the amount of lipid in the free-standing membrane region to increase, potentially increasing the amount of measurable protein during an experiment. Together, these insights should make it easier to measure and interpret the mechanical state of the membrane, although they also suggest the existence of multiple sources of uncontrolled variation in apparent channel behavior during electrophysiological experiments.

Acknowledgments
The authors thank Rod MacKinnon and Daniel Schmidt for stimulating discussion and critical reading of the early manuscript. We thank Paul Blount for kindly providing us with the membrane shape data. We are grateful for the following funding sources: T.U. for the Genentech Bio-X Postdoctoral Fellowship, and T.U., A.A. and R.P. for the NIH Director's Pioneer Award, the HHMI Collaborative Innovation Award and NIH Award number R01 GM084211.

References

[1] E. A. Evans. Bending elastic modulus of red blood cell membrane derived from buckling instability in micropipet aspiration tests. *Biophys J*, 43(1):27–30, 1983.

[2] E. Evans and A. Yeung. Apparent viscosity and cortical tension of blood granulocytes determined by micropipet aspiration. *Biophys J*, 56(1):151–60, 1989.

[3] P.S. Sit, A.A. Spector, A.J. Lue, A.S. Popel, and W.E. Brownell. Micropipette aspiration on the outer hair cell lateral wall. *Biophys J*, 72(6):2812–9, 1997.

[4] F. Guilak, J.R. Tedrow, and R. Burgkart. Viscoelastic properties of the cell nucleus. *Biochem Biophys Res Commun*, 269(3):781–6, 2000.

[5] A. Roux, D. Cuvelier, P. Nassoy, J. Prost, P. Bassereau, and B. Goud. Role of curvature and phase transition in lipid sorting and fission of membrane tubules. *Embo J*, 24(8):1537–45, 2005.

[6] A. Roux, G. Koster, M. Lenz, B. Sorre, J-B Manneville, P. Nassoy, , and P. Bassereau. Membrane curvature controls dynamin polymerization. *Proc Natl Acad Sci U S A*, 107(9):4141–6, 2010.

[7] P. Moe and P. Blount. Assessment of potential stimuli for mechano-dependent gating of mscl: effects of pressure, tension, and lipid headgroups. *Biochemistry*, 44(36):12239–44, 2005.

[8] D. Schmidt and R. MacKinnon. Voltage-dependent k+ channel gating and voltage sensor toxin sensitivity depend on the mechanical state of the lipid membrane. *PNAS*, 105(49):19275–19280, 2008.

[9] T. M. Suchyna, S. E. Tape, 2nd Koeppe, R. E., O. S. Andersen, F. Sachs, and P. A. Gottlieb. Bilayer-dependent inhibition of mechanosensitive channels by neuroactive peptide enantiomers. *Nature*, 430(6996):235–40, 2004.

[10] E. Perozo, A. Kloda, D. M. Cortes, and B. Martinac. Physical principles underlying the transduction of bilayer deformation forces during mechanosensitive channel gating. *Nat Struct Biol*, 9(9):696–703, 2002.

[11] R. Phillips, T. Ursell, P. Wiggins, and P. Sens. Emerging roles for lipids in shaping membrane-protein function. *Nature*, 459:379–385, 2009.

[12] S. I. Sukharev, W. J. Sigurdson, C. Kung, and F. Sachs. Energetic and spatial parameters for gating of the bacterial large conductance mechanosensitive channel, mscl. *J Gen Physiol*, 113(4):525–40, 1999.

[13] P. Wiggins and R. Phillips. Analytic models for mechanotransduction: gating a mechanosensitive channel. *Proc Natl Acad Sci U S A*, 101(12):4071–6, 2004.

[14] C.E. Morris and P.F. Juranka. Lipid stress at play: Mechanosensitivity of voltage-gated channels. *Curr Top Memb*, 49:298–338, 2007.

[15] C. E. Morris and U. Homann. Cell surface area regulation and membrane tension. *J Membr Biol*, 179(2):79–102, 2001.

[16] W. Rawicz, K. C. Olbrich, T. McIntosh, D. Needham, and E. Evans. Effect of chain length and unsaturation on elasticity of lipid bilayers. *Biophys J*, 79(1):328–39, 2000.

[17] A. Priel, Z. Gil, V.T. Moy, K.L. Magleby, and S.D. Silberberg. Ionic requirements for membrane-glass adhesion and giga seal formation in patch-clamp recording. *Biophys J*, 92:3893–3900, 2007.

[18] H. Schonherr, J.M. Johnson, P. Lenz, C.W. Frank, and S.G. Boxer. Vesicle adsorption and lipid bilayer formation on glass studied by atomic force microscopy. *Langmuir*, 20:11600–11606, 2004.

[19] L. R. Opsahl and W. W. Webb. Lipid-glass adhesion in giga-sealed patch-clamped membranes. *Biophys J*, 66(1):75–9, 1994.

[20] J. Dai and M. P. Sheetz. Membrane tether formation from blebbing cells. *Biophys J*, 77(6):3363–70, 1999.

[21] A. Upadhyaya and M. P. Sheetz. Tension in tubulovesicular networks of golgi and endoplasmic reticulum membranes. *Biophys J*, 86(5):2923–8, 2004.

[22] C. X. Gu, P. F. Juranka, and C. E. Morris. Stretch-activation and stretch-inactivation of shaker-ir, a voltage-gated k+ channel. *Biophys J*, 80(6):2678–93, 2001.

[23] C. E. Morris and P. F. Juranka. Nav channel mechanosensitivity: activation and inactivation accelerate reversibly with stretch. *Biophys J*, 93(3):822–33, 2007.

[24] B. Akitake, A. Anishkin, and S. Sukharev. The "dashpot" mechanism of stretch-dependent gating in mscs. *J Gen Physiol*, 125(2):143–54, 2005.

[25] E. Evans, V. Heinrich, F. Ludwig, and W. Rawicz. Dynamic tension spectroscopy and strength of biomembranes. *Biophys J*, 85(4):2342–50, 2003.

[26] D. Boal. *Mechanics of the Cell*. Cambridge University Press, 1st edition, 2002.

[27] E. Evans. Entropy-driven tension in vesicle membranes and unbinding of adherent vesicles. *Langmuir*, 7:1900–8, 1991.

[28] U. Seifert and R. Lipowsky. Adhesion of vesicles. *Physical Review. A*, 42(8):4768–71, 1991.

[29] A.-S. Smith, E. Sackmann, and U. Seifert. Pulling tethers from adhered vesicles. *Phys Rev Lett*, 92(20):208101, 2004.

[30] A.-S. Smith, B.G. Lorz, S. Goennenwein, and E. Sackmann. Force-controlled equilibria of specific vesicle-substrate adhesion. *Biophys J*, 90(7):L52–4, 2006.

[31] T. M. Suchyna, V. S. Markin, and F. Sachs. Biophysics and structure of the patch and the gigaseal. *Biophys J*, 97:738–747, 2009.

Pressure (mm Hg)	Method 1 $\tau = pR_c/2$	Method 2 $\tau = \sqrt{\gamma^2 + (pR_p/2)^2}$	Method 3 $\tau = \gamma + pR_p/2$
24	na	0.98	1.29
42	na	1.13	1.58
72.7	na	1.48	2.07

Table 1: Estimation of gating tension (in k_BT/nm^2) for methods 2 (Opsahl and Webb [19]) and 3 (this work) using data from [10]. ('na' - not available)

Captions:

Figure 1: Schematic of the pipette and membrane geometry. The two figures illustrate the cases of (a) zero and (b) non-zero pressure, with the relevant geometric parameters for a cylindrical pipette.

Figure 2: Plots showing the non-dimensional variables under pressure. a) The dimensionless tension $\hat{\tau} = \tau/\gamma$ for the method developed here (solid line, Method 3: $\tau = \gamma + pR_p/2$), and the method of Opsahl and Webb [19] (dashed line, Method 2: $\tau = \sqrt{(pR_p/2)^2 + \gamma^2}$), both of which do not require knowledge of membrane curvature. b) The dimensionless curvature $\rho = R_p/R_c$ as a function of the dimensionless pressure $\hat{p} = pR_p/2\gamma$, from eqn. 15.

Figure 3: Plots showing free-standing area and adherence length with dimensionless pressure. a) The fractional change of lipid in the free-standing region as a function of dimensionless pressure, for $\phi_o = 0.01$. Under pressure the free-standing region may gain up to $\sim 20\%$ more lipid. For reference, the areal strain of the membrane is shown as a dashed line. b) Plots of the length of the adhered region relative to the pipette radius for the membrane areas ($A_o/\pi R_p^2$) noted and $\phi_o = 0.01$. As demonstrated by these plots, the contact boundary defined by L_p can move in a non-monotonic fashion depending on the membrane area. c) Precise schematic of membrane shape evolution under pressure, for a cylindrical pipette with $R_p = 1\,\mu$m and $A_o = 2\pi R_p^2$ (bottom of (b)). The red region is the lipids originally in the free standing region at zero pressure. d) Zoom in of box in (c) showing membrane moving from the adhered region into the free standing region.

Figure 4: Glass-bilayer adhesion measured in different bilayer mixtures. Measurements of patch curvature as a function of applied pressure can be fit to eqn. 14 to find values of the adhesion energy, γ, from the slopes of the lines. Variations in adhesion strength between different lipid mixtures may be due to head group chemistry, and overall variations in adhesion strength may be due to differences in pipette glass or buffer conditions [17]. Graphs (a) through (e) use data from [7]; graph (f) uses data from [19]. The different colors in a plot correspond to different data sets for a particular lipid type.

Figure 5: Bar graph comparing the strength of adhesion between the different lipid mixtures shown in Fig. 4. The means and standard deviations come from the linear slopes of the fits to each data set.

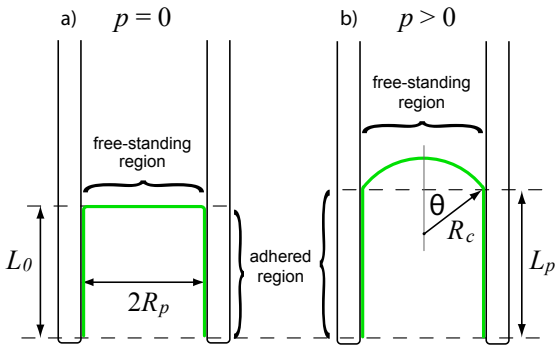

Figure 1:

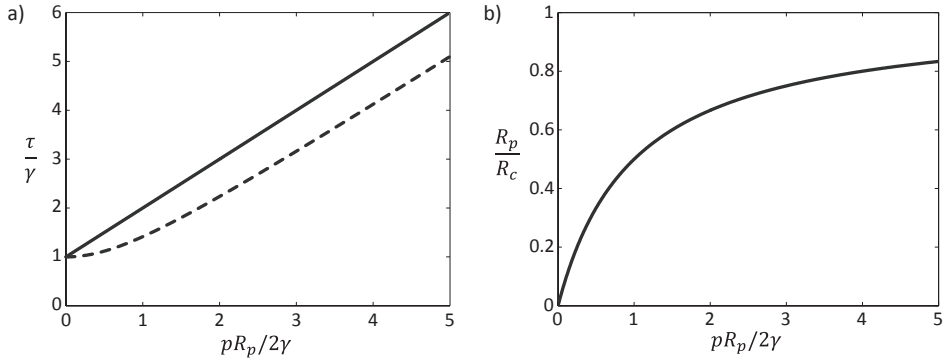

Figure 2:

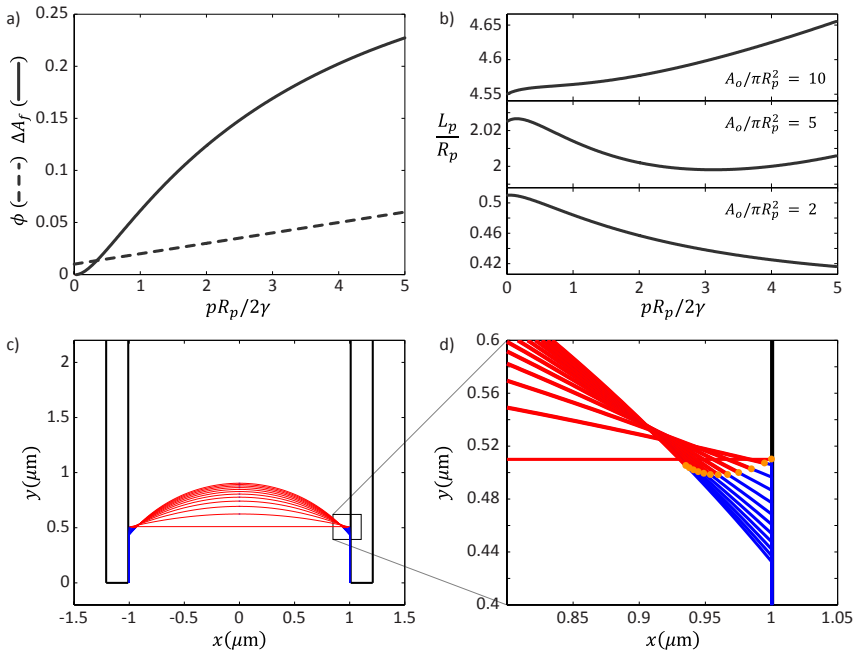
a)
b)
c)
d)
ϕ (- - -) ΔA_f (——)
$pR_p/2\gamma$
$\frac{L_p}{R_p}$
$A_o/\pi R_p^2 = 10$
$A_o/\pi R_p^2 = 5$
$A_o/\pi R_p^2 = 2$
$y(\mu m)$
$x(\mu m)$

Figure 3:

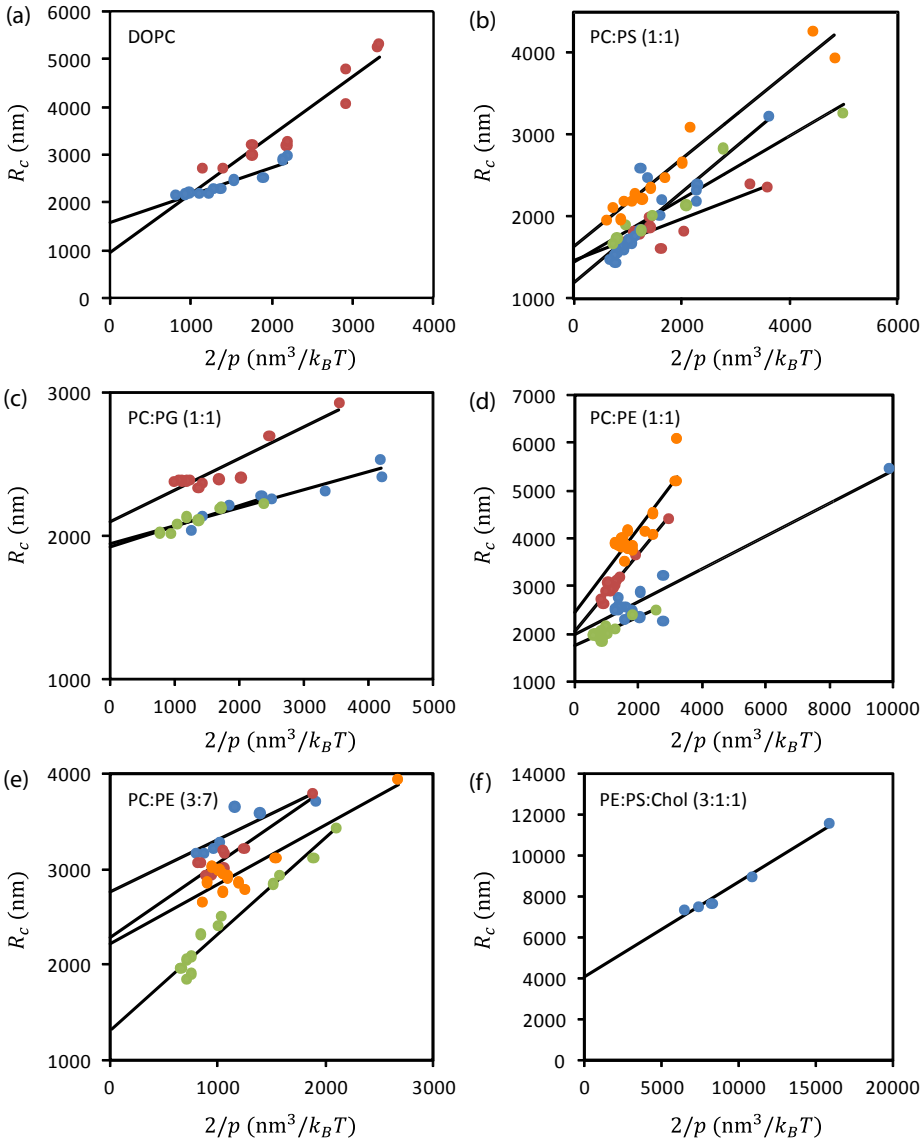
(a)
DOPC
R_c (nm)
$2/p$ (nm$^3/k_BT$)
(b)
PC:PS (1:1)
(c)
PC:PG (1:1)
(d)
PC:PE (1:1)
(e)
PC:PE (3:7)
(f)
PE:PS:Chol (3:1:1)

Figure 4:

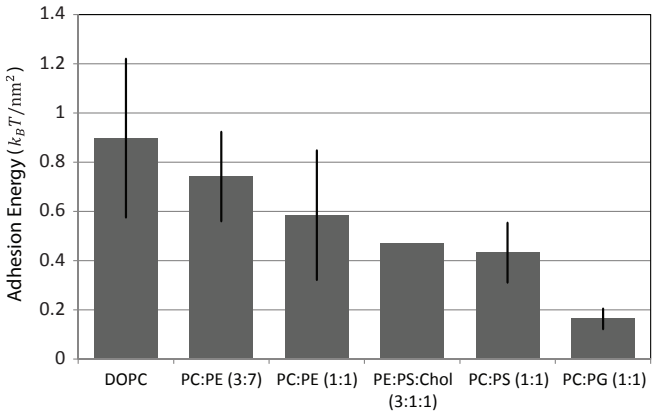
1.4
1.2
1
0.8
0.6
0.4
0.2
0
Adhesion Energy (k_BT/nm^2)
DOPC
PC:PE (3:7)
PC:PE (1:1)
PE:PS:Chol (3:1:1)
PC:PS (1:1)
PC:PG (1:1)

Figure 5: